International Journal of Dynamics and Control
https://doi.org/10.1007/s40435-023-01164-y

A study on a computationally efficient controller design for a surgical robotic system

Orhan Ayit[1] · **Mehmet İsmet Can Dede**[1]

Received: 27 September 2022 / Revised: 13 February 2023 / Accepted: 11 March 2023

Abstract
The control algorithms of the surgical robotic system using the robot's dynamics produce a relatively high computational load on the processor. This paper develops a computationally efficient computed torque controller by using a simplified dynamic modeling method and implemented in a novel surgical robot experimentally. In addition, an independent joint controller is designed and implemented to compare the results of the computed torque controller.

Keywords Simplified dynamic model · Computed torque method · Independent joint controller

1 Introduction

In the 1980s, minimally invasive surgery (MIS) emerged as a type of surgery. It was performed by inserting medical instruments and a camera (called the endoscope) through one or more small incisions or the natural orifice. It is preferred due to its advantages over open surgeries, such as no or fewer incisions, short recovery time, decreased infection risk, reduced blood loss, and fewer complications [1, 2]. Despite these advantages, requiring special training, increasing the surgery duration, limited mobility/maneuverability, physical fatigue, and requiring more concentration are the disadvantages over open surgeries [3, 4]. To deal with the issues, the robots have been used in MIS, and by that way, the range of motion, dexterity, and visualization is increased; moreover, the physical and physiological stress on surgeons are eliminated [5–7]. Due to these benefits of the robots on the surgeons and patients, robots are being used in surgeries related to urology, cardiovascular, gynecology, otolaryngology, thyroid, colorectal diseases, obesity, and general surgery [8].

Attanasio, A. et al. categorized surgical robots according to their autonomy level 0 to 5 [9] where surgical robots in level 0 are not autonomous such as [12–14], and each action performed by them is dependent on the surgeons' commands. In contrast, the robots in level 5 have full autonomy and they can complete the surgery without any supervision or planning made by the surgeon. However, there is no fully autonomous surgical robot in literature as reported in [9]. As the autonomy level increases, the surgical robots gain multiple functionalities such as perceiving the surgical scenario and environment by using multiple sensors, generating/updating the new trajectory paths, and making the decision in addition to following the motion trajectories precisely. Implementing the algorithms for obtaining these functions results in extensive computational costs on the surgical robots' main processor. To deal with this issue, computationally efficient algorithms are required to be implemented in the surgical robots' processor. For instance, Zhang L. and Yang G.Z presented a relatively simple and computationally efficient iterative method to solve the hand-eye calibration problem for image-guided surgical robots [16]. In [17], a physics-based tracking approach was proposed, which provides a surgical robot to follow the heart surface with sufficiently low computational time for using it in real-time beating heart surgery robotic systems. Moreover, motion control algorithms cause high computational costs on the processor since they are run at high frequencies. The well-known motion controllers, such as adaptive or computed torque controller, use the full or partial mathematical dynamic model of the robot, which result in high computational costs. Therefore, this study focuses on computationally efficient motion controller design.

✉ Orhan Ayit
orhanayit@iyte.edu.tr

Mehmet İsmet Can Dede
candede@iyte.edu.tr

[1] Department of Mechanical Engineer, Izmir Institute of Technology, İzmir, Türkiye

Published online: 17 April 2023

In the literature, two main approaches for formulating the rigid body dynamics of the robot are the Newton–Euler approach and the Lagrange formulation. Featherstone stated that the computational complexity of both methods is drastically decreased when the recursive formulation is applied rather than the non-recursive formulation [18]. Other traditional rigid body dynamic methods are the virtual work, the Hamilton, and the Kane principles. Deriving the complex surgical robot's rigid body dynamics for implementing the motion control algorithm in the low-cost embedded system cannot be computationally efficient enough by using these methods. The simplification methods for the dynamic models were studied to reduce the computational time. In [19], the influence of the terms related to velocity and acceleration for the Delta parallel manipulator are investigated, and the terms that have an insignificant effect on the dynamic model are neglected to decrease the computational time. Brinker et al. proposed a simplified approach for the Delta parallel robot, which has relatively slow motion in [20] where the velocity of the joints, attached to distal and proximal links, and rotational inertia of the distal links are neglected. In [22], the interval method is applied to simplify the robot dynamics to reduce the computational time and memory allocation. Carbonari proposed a new simplified dynamic model approach based on fitting a translational Cartesian manipulator dynamic by using approximated polynomial functions [24]. In [26], Gao et al. stated that the dynamics related to the legs of the 3-PRRR/PPRR redundant mechanism results in complexity in the model. To simplify the dynamics, link masses are separated into two-part and added to the mass of the moving platform and sliders, respectively.

The main contribution of this study is to develop a computationally efficient motion controller architecture in surgical robotic systems. Preliminary studies of this paper were presented in [28, 29] where a simplified dynamic model with a novel correction coefficient formula was proposed and verified in the simulation environment. This paper combines the proposed simplified dynamic model with a computed torque controller for controlling a parallel surgical robot with the remote center of motion mechanism named as NeuRoboScope. This robot was designed in Human–Robot Interaction Laboratory (HuR) in the Izmir Institute of Technology for assisting a minimally invasive endoscopic pituitary tumor surgery. In addition to the computed torque controller, an independent joint controller with simplified gravity compensation is implemented in NeuRoboScope, and the performance of both controllers is compared and discussed based on their experimental results.

The rest of the paper is organized as follows: Section 2 represents the mathematical models including kinematics and dynamics of the NeuRoboScope. In Sect. 3, the design of the simplified dynamic model with the novel correction coefficient formula is reviewed. Section 4 provides the design of the controllers such as computed torque and independent joint controllers. Section 5 provides and examines the main results, i.e., the performance of the computed torque and independent joint controllers. Section 6 concludes the paper.

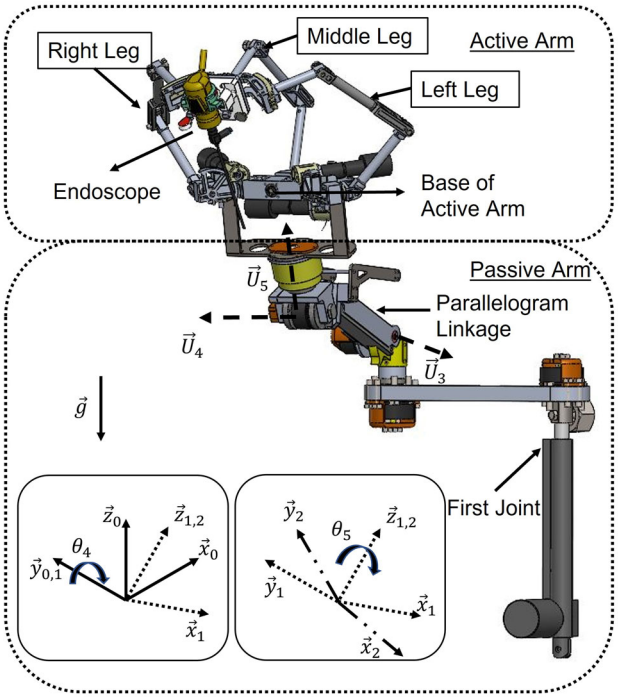

Fig. 1 The representation of the passive (left side) and active (right side) arms of the NeuRoboScope

2 Mathematical models of the NeuRoboScope

2.1 Kinematic Model

NeuRoboScope surgical robot integrates a parallel (active arm) and serial (passive arm) manipulator as shown in Fig. 1.

The tip of the passive arm is directly connected to the active arm's base. The passive arm is a serial manipulator that carries and adjusts the position of the active arm's base to the operating table. The first joint of the manipulator is an active prismatic joint that regulates the robot's elevation. The other joints of the manipulator are revolute and backdrivable. A brake and an absolute encoder are attached to each revolute joint to lock the joints and measure the orientation and position of the tip of the passive arm, respectively. As observed in Fig. 1, the fourth (rotate around $\mathbf{U}_4$) and the fifth (rotate around $\mathbf{U}_5$) revolute joints are responsible for the orientation of the tip of the passive arm, and the third (rotate around $\mathbf{U}_3$) revolute joint does not have an effect on the orientation due to parallelogram linkage mechanism. Revolute joints, except the fourth and the fifth ones, provide translation motion of

the passive arm's tip. The rotation around $\mathbf{U}_4$ is sufficient to reach the entire surgical workspace by the NeuRoboScope, while the rotation around $\mathbf{U}_5$ provides ergonomic usage for the surgeon. The orientation of the tip of the passive arm (base of the active arm) is derived by using a rotation angle around $\mathbf{U}_4$ (θ_4) and $\mathbf{U}_5$ (θ_5). The frames are defined as $\mathbf{F}_0$ attached to the world frame and $\mathbf{F}_2$ attached to the base of the active arm, which are coincident when $\theta_4 = 0°$ and $\theta_5 = 0°$. $\mathbf{y}_1$ and $\mathbf{y}_0$ are coincident when $\theta_4 = 0°$ and $\mathbf{z}_1$ and $\mathbf{z}_2$ are coincident when $\theta_5 = 0°$ as observed in Fig. 1. The rotation matrix is indicated as $\hat{R}_0^2$ for rotating $\mathbf{F}_0$ to $\mathbf{F}_2$.

The function of the active part is holding and controlling the endoscope, located at the tip of this manipulator, which has three degrees of freedom parallel kinematic structure with a remote center of motion (RCM) mechanism. Figure 2 indicates RCM as a point P where $\mathbf{W}$ is defined by points P and P_{M3} (that coincident with P_{L3} and P_{R3}). Also, the $\mathbf{W}$ represents the endoscope. The generalized coordinates of the active parts in joint space are θ_1, θ_2 and θ_3 that are used to control the two rotational (ϕ & ψ) and a translational motion (d). ϕ refers to an angle defined between $\mathbf{W}$ and $\mathbf{XZ}$ plane, while ψ refers to an angle defined between $\mathbf{W}$ and $\mathbf{YZ}$ plane. Also, d is defined as a distance between points P and P_{M3} along $\mathbf{W}$. The motion range of ϕ, ψ and d are 30° (−15° to 15°), 40° (−20° to 20°) and 100 mm (150 mm to 250 mm), respectively. l_0 is chosen as 200 mm. To make the condition number of the mechanism within its workspace close to 1 for reaching the best force transmission characteristic, the kinematic parameters μ_1, μ_2, and β are designed as $\frac{\pi}{4}$ rad, $-\frac{\pi}{4}$ rad, and 0 rad in [31]. In this previous study, the derivation of forward and inverse kinematic models of the NeuRoboScope is presented in detail. As explained in [32], a manipulator is close to a singular configuration when the condition number gets very large values. By designed μ_1, μ_2, and β, the singularity of the NeuRoboScope is avoided in its specified workspace.

In Fig. 2, the frame attached to the endoscope is defined as $\mathbf{F}_3$ in which $\mathbf{W}$ and $\mathbf{z}_3$ are coincident. A rotation matrix depends on rotation angles around $\mathbf{x}_3$ (θ_x) and $\mathbf{y}_3$ (θ_y) is derived as $\hat{R}_2^3$ for rotating $\mathbf{F}_2$ to $\mathbf{F}_3$. $\mathbf{F}_2$ and $\mathbf{F}_3$ are coincident when $\theta_x = 0°$ and $\theta_y = 0°$. It is noted that θ_x and θ_y are not the same as ϕ and ψ.

The relation between task space variable $\bar{\Gamma} = \begin{bmatrix}\phi & \psi & d\end{bmatrix}^T$ and joint space variable $\bar{\theta} = \begin{bmatrix}\theta_1 & \theta_2 & \theta_3\end{bmatrix}^T$ can be found in [30]. At the velocity level, the relation between the velocity of the task and joint variables is derived by using a Jacobian matrix $\hat{J}_n$ as represented below.

$$\dot{\bar{\Gamma}} = \hat{J}_n \dot{\bar{\theta}} \tag{1}$$

Another Jacobian matrix $\hat{J}$ is defined to relate the variables $\dot{\bar{\rho}}$ (where $\rho = \begin{bmatrix}\theta_x & \theta_y & d\end{bmatrix}^T$) to velocities of the joint space variables $\dot{\bar{\theta}}$ as represented below.

$$\dot{\bar{\rho}} = \hat{J}\dot{\bar{\theta}} \tag{2}$$

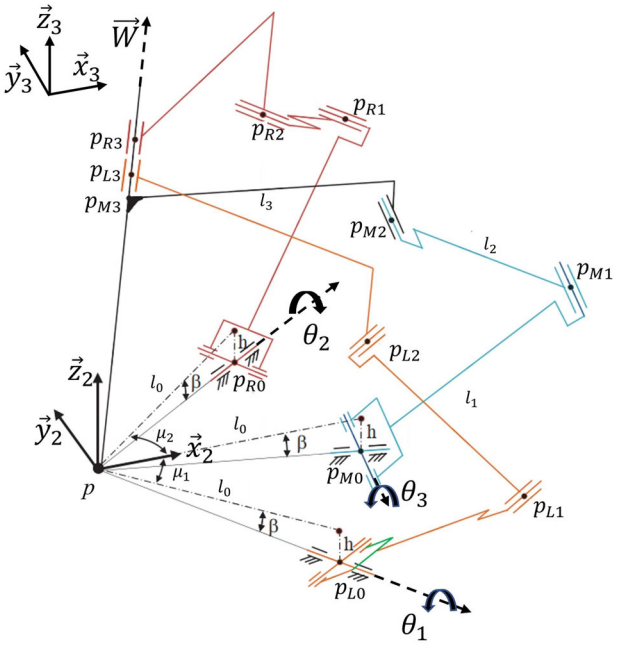

Fig. 2 The representation of the kinematic diagram of the active arm of the NeuRoboScope [30]

Table 1 The kinematic and inertial parameters of the NeuRoboScope

Leg	Links	Link Length (mm)	Distance btw CoM and Joint (mm)	Mass (gr)
Left	1^{st}	135	75.6	73.3
	2^{nd}	195	107.4	115.8
	3^{rd}	200	65.6	111.3
Right	1^{st}	135	75.8	74.3
	2^{nd}	195	107.2	116.1
	3^{rd}	200	75.4	112.1
Middle	1^{st}	135	44.82	159.7
	2^{nd}	195	111.5	93.6
	3^{rd}	200	114.2	361.9
Endoscope		250	36.7	797.2

The kinematic and inertial parameters such as length, location of the center of mass (CoM), and mass of links are presented in Table 1, which is used in dynamic studies of the robot. Detailed information about the kinematic model can be found in [30].

2.2 Dynamic model

The rigid body dynamic model is presented as follows.

$$\bar{T} + \bar{T}_d = \hat{M}(\bar{q})\ddot{\bar{q}} + \hat{C}(\dot{\bar{q}}, \bar{q})\dot{\bar{q}} + \bar{G}(\bar{q}) \tag{3}$$

where $\hat{M} \in \mathbb{R}^{3\times3}$, $\hat{C} \in \mathbb{R}^{3\times3}$ and $\bar{G} \in \mathbb{R}^{3\times1}$ refer to the mass matrix, Coriolis and centrifugal matrix, and gravitational torque column matrix, respectively. The generalized coordinate, applied torque, and disturbance torque column matrices are indicated as $\bar{q} \in \mathbb{R}^{3\times1}$, $\bar{T} \in \mathbb{R}^{3\times1}$, and $\bar{T}_d \in \mathbb{R}^{3\times1}$. Since the NeuRoboScope's active part has three degrees of freedom, generalized coordinates can be chosen as three independent joint or task space variables. In this study, the actuated joint variables (θ_1, θ_2, θ_3) shown in Fig. 2 are used as generalized coordinates. Therefore, $\bar{q} = \begin{bmatrix}\theta_1 & \theta_2 & \theta_3\end{bmatrix}^T$ and $\bar{T} = \begin{bmatrix}T_1 & T_2 & T_3\end{bmatrix}^T$. T_1, T_2, and T_3 are applied torque by the actuators coupled to right, left, and middle leg, respectively. $\bar{T}_d$ is the effects of the passive joint frictions imposed on the actuated joints. Moreover, the applied torques on the actuated joints $\bar{T}$ can be explicitly defined as below.

$$\bar{T} = \bar{T}_{\text{act}} - \bar{T}_{\text{fric}} \tag{4}$$

$\bar{T}_{\text{act}} \in \mathbb{R}^{3\times1}$ refers torques generated from the actuators and $\bar{T}_{\text{fric}} \in \mathbb{R}^{3\times1}$ is the resistive torques due to the friction of actuation system (due to mainly the speed reduction system).

The dynamics of the NeuRoboScope are investigated as the active arm's dynamics by neglecting the passive arm's dynamics because the joints of the passive arm, except the first joint, are passive, and the first joint is only used at the beginning of the surgery. The dynamics of the NeuRoboScope are derived using the recursive Newton–Euler algorithm, and the algorithm is embedded in ARM Cortex M4, which has high performance and cost-efficiency. It is observed that the processor requires the undesired high computational time to run even a tiny part of the algorithm. To deal with the issue, the effect of acceleration, velocity, and gravitational terms on the dynamics of the NeuRoboScope is investigated in a simulation environment by using the Multibody library in MATLAB/Simulink. This library allows the model of the robot to follow the given position, velocity, and acceleration trajectories independently. By taking advantage of this feature, the obtained torque values from NeuRoboScope's models (i) following the joint velocity and acceleration trajectories given as zero, while correct gravitational acceleration is given, (ii) following the joint velocity trajectories given as maximum value and joint acceleration trajectories given as zero, (iii) following the joint acceleration trajectories given as maximum value and joint velocity trajectories given as zero are compared with the torque values from the model, (iv) following the maximum joint velocity and acceleration trajectories with correct gravitational acceleration when scanning the workspace of the NeuRoboScope. In (ii) and (ii), the gravitational acceleration is given as $\mathbf{0}\ \frac{m}{s^2}$. As observed in Eq. 3, acceleration, velocity, and gravity are directly related to mass, Coriolis and centrifugal, and gravitational torque column matrices, respectively. Therefore, the effects of $\hat{G}(\bar{q})$, $\hat{M}(\bar{q})$, $\hat{C}(\bar{q}, \dot{\bar{q}})$ on the dynamics of the NeuRoboScope are investigated by a using the models (i–iii), separately. Moreover, the torques due to the complete dynamics of the robot are obtained from model (iv). The maximum velocity and acceleration values are derived as 2 $\frac{\text{rad}}{s}$ and 7.4 $\frac{\text{rad}}{s^2}$ from the workspace studies of the NeuRoboScope [33]. The average percentage of the obtained torques from models (i–iii) according to obtained torques from the model (iv) is presented in Fig. 3 where the average percentage of torques due to gravitational acceleration, inertial torques, and Coriolis and centrifugal torques of total torques is obtained as 75.5%, 11.5%, and 13%, respectively.

3 Simplified dynamic model

Formerly, the analysis of the NeuRoboScope's dynamic model was done where the results imply that gravitational acceleration has a dominant effect on the NeuRoboScope's dynamics, while the effect of the inertial and Coriolis and centrifugal terms on the dynamics is approximately the same. Moreover, workspace studies show that the maximum joint velocities are rarely reached during the surgical operation. In addition, Table 1 indicates that the mass of the endoscope has relatively higher effects on the dynamics when compared with links' mass. According to these inferences from the analysis, the assumptions mentioned in [28, 29] are made for modeling the NeuRoboScope's dynamics.

- The NeuRoboScope is assumed as a rigid parallel manipulator.
- The frictional effects are neglected because the actuation system of NeuRoboScope shown in Fig. 6 has a relatively high reduction ratio 1 : 905. The effect of the passive joint frictions becomes insignificant as they are reflected to the actuator that has a large gear reduction ratio ($\bar{T}_d = \bar{0}$).
- $\hat{C}(\bar{q}, \dot{\bar{q}})$ is neglected due to not reaching the maximum speed during operation, and the speed-dependent terms have a relatively lower effect on the NeuRoboScope's dynamics.
- The masses of NeuRoboScope's parts (such as links and actuators) except the endoscope are neglected.
- The inertia of the NeuRoboScope's parts, except the endoscope and an actuator attached to the middle leg, is neglected.

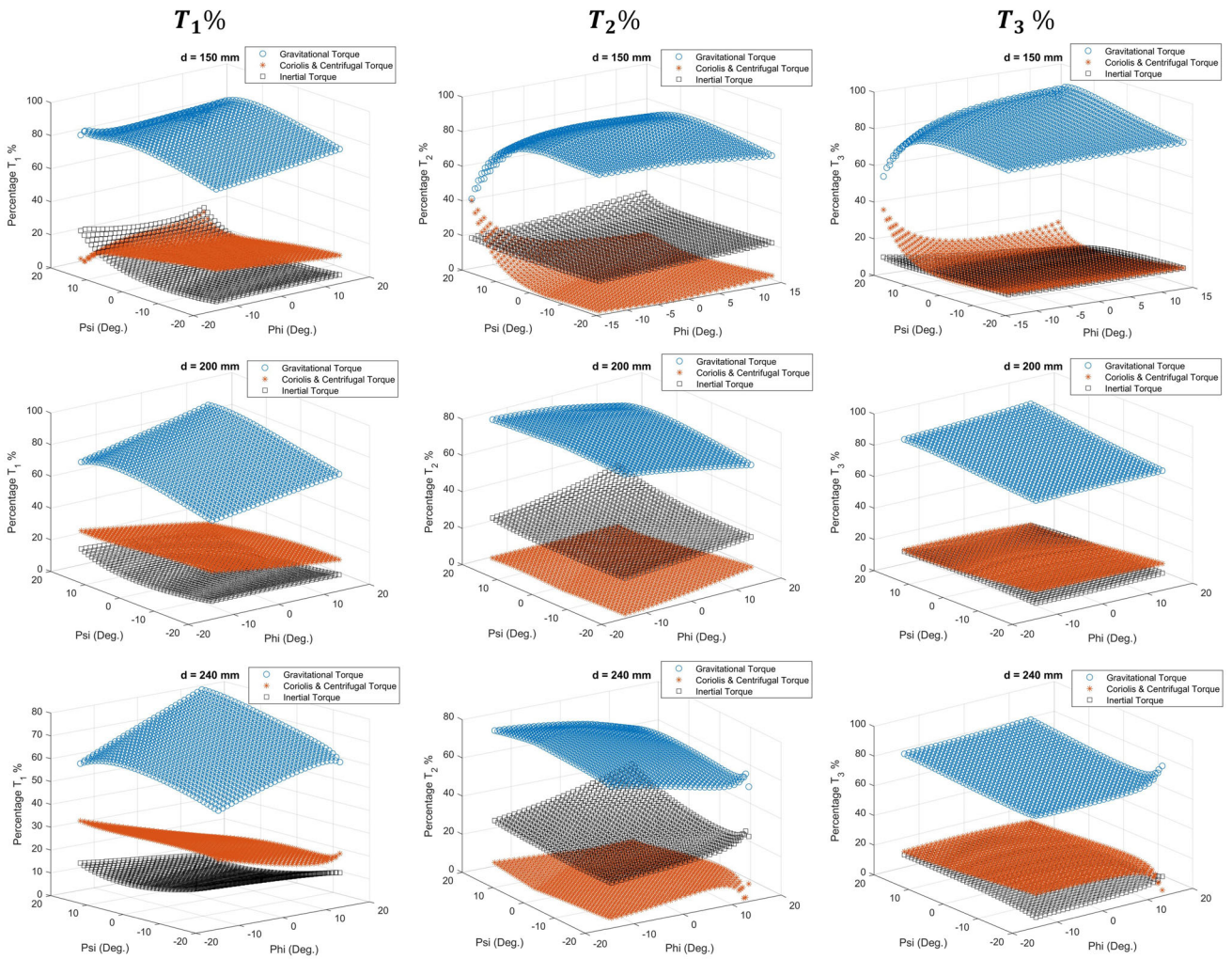

Fig. 3 The percentage value of the inertial, Coriolis and centrifugal and gravitational torques of the total torques $T1$, T_2 and T_3 when ϕ is increased by 1 from $-14°$ to $14°$, ψ is increased by 1 from $-14°$ to $14°$ and $d = 150$, 200 and 240 mm

By using these assumptions, the rigid body dynamic model is modified as follows:

$$\bar{T} = \hat{K}_{\text{corr}}[\tilde{M}(\bar{q})\ddot{\bar{q}} + \tilde{G}(\bar{q})] \tag{5}$$

where $\hat{K}_{\text{corr}}$, $\tilde{M}(\bar{q})$ and $\tilde{G}(\bar{q})$ refer to correction coefficient, simplified mass matrix and simplified gravitational torque column matrix, respectively. Moreover,

The simplified mass matrix is calculated as follows.

$$\begin{aligned} \tilde{M} &= \hat{M}_x + \hat{M}_\theta \\ \hat{M}_x &= \hat{\mathrm{J}}_n^T(\tilde{V}_{end})^T m_{end} \tilde{V}_{end} \hat{\mathrm{J}}_n \\ \hat{M}_\theta &= \hat{\mathrm{J}}_w^T((\hat{R}_2^1)\hat{I}_{end}(\hat{R}_2^1)^T + \hat{I}_{act})\hat{\mathrm{J}}_w \end{aligned} \tag{6}$$

where m_{end}, $\hat{I}_{end}$, and $\bar{L}_{end}$ denote the mass, inertia defined in $\mathbf{F}_3$ and CoM of the endoscope.

$\hat{\mathrm{J}}_w$ is a redundant Jacobian matrix, and it is obtained by substituting the elements of the third row of $\hat{J}$ by zero. The $\hat{I}_{act}$ defined in $\mathbf{F}_2$ refers to actuator's inertia. Also, first element of $\hat{I}_{act}$ is equal to $14.81 \times 10^{-7}\, kgm^2$ and other elements are equal to zero. In addition, $\tilde{V}_{end}$ is calculated as:

$$\bar{V}_{end} = \tilde{V}_{end} \begin{bmatrix} \dot{\phi} \\ \dot{\psi} \\ \dot{d} \end{bmatrix} \tag{7}$$

where $\bar{V}_{end} = \frac{d(\hat{R}_2^1 \bar{L}_{end})}{dt}$.

According to these assumptions, the gravitational torques are generated due to the endoscope's weight. The simplified gravitational torque column matrix is calculated using the virtual work method, as shown below.

$$\bar{G}_s(q) = -\hat{\mathrm{J}}^T \bar{F} \tag{8}$$

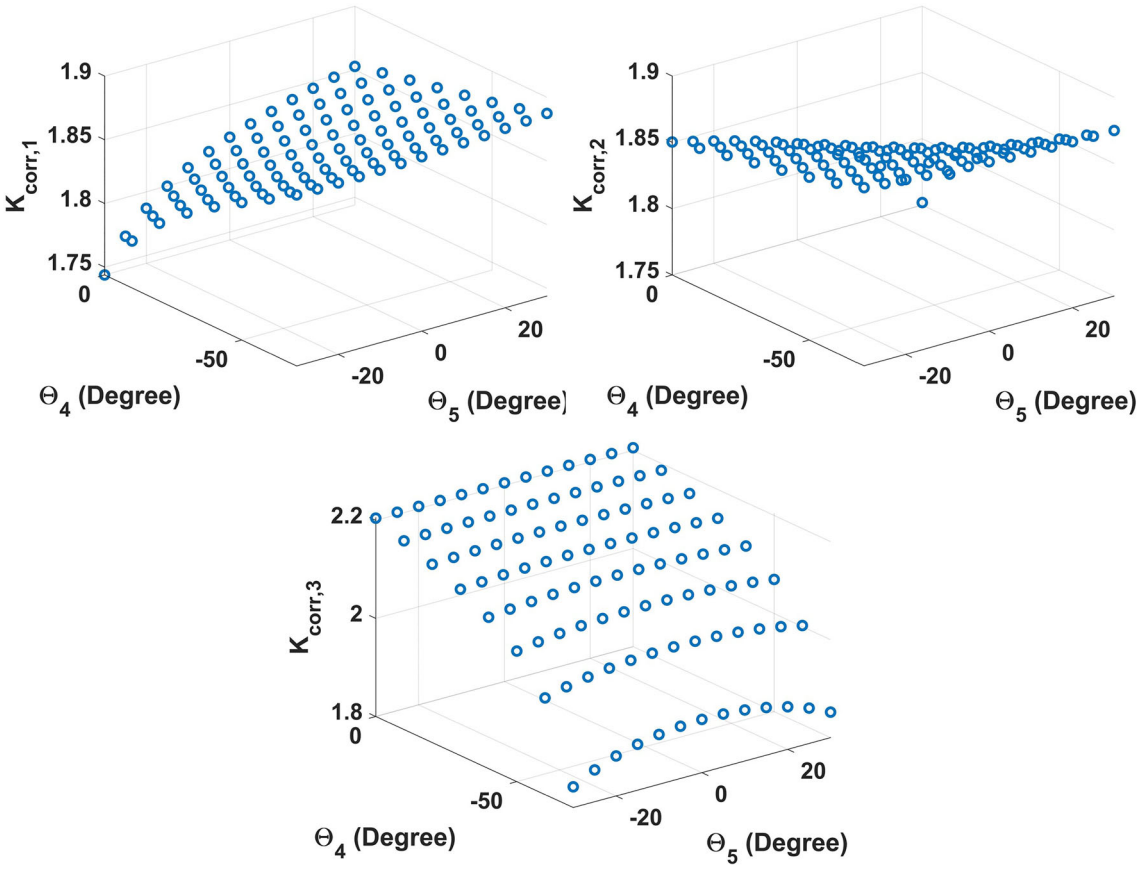

Fig. 4 The calculated correction coefficient values according to θ_4

The correction coefficient $\hat{K}_{\text{corr}}$ matrix is a diagonal matrix consisting of $\hat{K}_{\text{corr},1}$, $\hat{K}_{corr,2}$ and $\hat{K}_{corr,3}$ which are used for correcting the torques T_1, T_2, T_3 obtained from the simplified dynamic model, respectively, and the correction coefficients are varied according to θ_4 and θ_5 which get value between 0° to −70° and −30° to 30°, respectively. The detailed information on deriving the $\hat{K}_{corr}$ can be found in [29]. The correction coefficients for the NeuRoboScope's dynamics are calculated for different θ_4 and θ_5 values as shown in Fig. 4.

By choosing the different θ_4 and θ_5 values, the simulations are done by using Simulink/MATLAB, where the simplified dynamic model with correction coefficient is compared with the NeuRoboScope's accurate dynamic model when the robot follows the motion trajectory shown in Fig. 5. In Table 2, the root-mean-square errors (RMSEs) between torques obtained from the simplified and accurate dynamic model of the NeuRoboScope are presented. The RMSEs are relatively small compared to the maximum torque values, which shows that the simplified dynamic model can be used instead of the actual dynamic model of the NeuRoboScope.

4 Design of the motion controllers

4.1 Actuation system's dynamics

The dynamics of the actuation have an important role in the design of the controller. NeuRoboScope has three identical actuation systems, which contain a DC motor (Maxon RE 25 Ø25 mm, Graphite Brushes, 20 Watt), a 181:1 planetary gearhead (Maxon GP 26 A Ø26 mm), a 5:1 capstan drive mechanism, a magnetic encoder to measure the output shaft of the gearhead (MagAlpha MA707 Absolute Encoder) and a magnetic brake (Maxon Brake AB 28) as shown in Fig. 6.

The transfer function of the motor dynamics is presented as follows.

$$\frac{\dot{\theta}_m(s)}{T_m(s)} = \frac{K_m}{(\tau_m s + 1)} \tag{9}$$

where $K_m \approx 131.9$ and $\tau_m \approx 0.035\ s$. θ_m and T_m refer to the measured angular speed of the output shaft of the gearhead and applied torque of the DC motor, respectively.

K_m and τ_m contain the viscous friction term η of the actuation system as discussed in [34]. By using the motor dynamic parameters, for achieving the best possible performance of

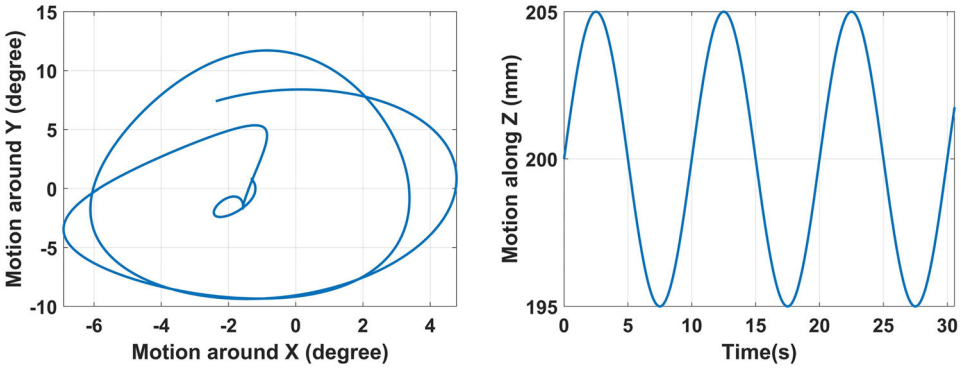

Fig. 5 The motion trajectory of the simulations. **X**, **Y** & **Z** - directions are defined in $\mathbf{F}_2$

Table 2 The RMSEs and maximum torques obtained from the simulation when $\theta_4 = -10°,-40°, -70°$. and $\theta_5 = 30°,0°, -30°$

θ_4°	θ_5°	Correction coefficients			RMSE (Nm)			Maximum torques (Nm)		
–	–	$K_{\text{corr},1}$	$K_{\text{corr},2}$	$K_{\text{corr},3}$	T_1	T_2	T_3	T_1	T_2	T_3
−10	–30	1.78	1.85	2.18	0.0544	0.0284	0.0320	2.4965	4.4594	2.5621
−40	–30	1.83	1.86	2.10	0.0337	0.0359	0.0522	3.1542	4.6899	2.0498
−70	–30	1.87	1.88	1.84	0.0245	0.0363	0.0874	3.1699	3.9058	1.2089
–10	0	1.83	1.83	2.18	0.0193	0.0192	0.0377	3.8817	3.9943	2.8390
−40	0	1.85	1.85	2.12	0.0164	0.0154	0.0505	4.2109	4.3234	2.3086
−70	0	1.88	1.88	1.9	0.0289	0.0268	0.0807	3.6612	3.7174	1.3330
−10	30	1.85	1.78	2.18	0.0268	0.0520	0.0326	4.4250	2.5759	2.6030
−40	30	1.87	1.83	2.11	0.0378	0.0302	0.0477	4.6670	3.2454	2.1036
−70	30	1.88	1.87	1.85	0.0415	0.0170	0.0855	3.9018	3.2430	1.2266

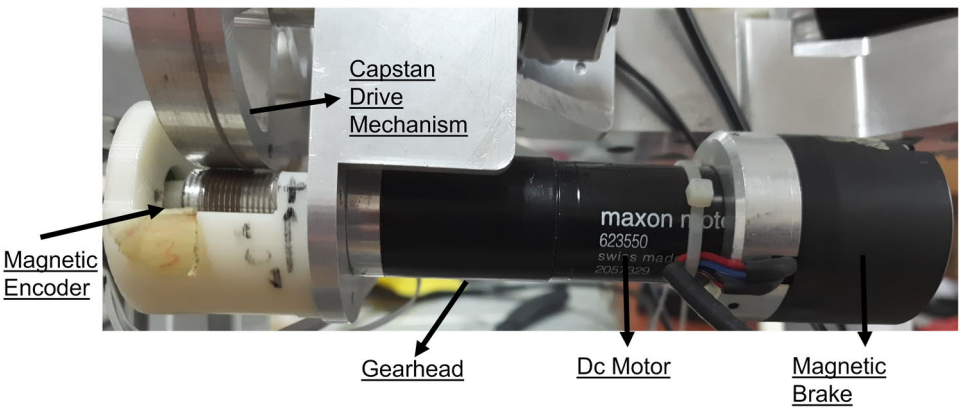

Fig. 6 The actuation system of the NeuRoboScope

the system, damping ratio ζ and natural frequency w_n are determined. For allowing the system to reach the desired steady-state response without oscillation and overshoot, the ζ is chosen as 0.707. Settling time with 2% tolerance of its steady-state response is formulated in Eq. 10, where the settling time τ_s is equal to four times τ_m ($\tau_s = 4\tau_m$).

$$\tau_s = \frac{4}{\zeta w_n} \tag{10}$$

According to Eq. 10, w_n is calculated as $\approx 40\frac{\text{rad}}{s}$.

By using the performance metrics ζ and w_n, the controller parameters are derived in section 4.2 and 4.3. Therefore, in the design of controllers, actuation system friction denoted as $\bar{T}_{fric}$ in Eq. 4 is taken into account.

4.2 Design of the Computed Torque Controller

As mentioned in Sect. 4.1, the actuation system has a 905:1 (181:1 + 5:1) reduction ratio; in addition, the angular velocity of the gear's output shaft is measured by the encoder. The position tracking error column matrix $\bar{e}$ is defined as follows:

$$\bar{e} = \bar{q}_m^{des} - \bar{q}_m \tag{11}$$

where $\bar{q}_m^{des}$ and $\bar{q}_m$ refer to desired angular position and measured angular joint position column matrix of the gear's output shaft.

The closed-loop error system is defined as:

$$\ddot{\bar{e}} + \hat{K}_d^{ct}\dot{\bar{e}} + \hat{K}_p^{ct}\bar{e} = \bar{0} \tag{12}$$

where $\hat{K}_d^{ct} = K_d^{ct}\hat{1}$ and $\hat{K}_p^{ct} = K_p^{ct}\hat{1}$ are controller coefficients, and $K_d^{ct} = 2\zeta w_n$ and $K_p^{ct} = w_n^2$.

By using the simplified dynamic model with correction coefficient shown in Eq. 5, the computed torque controller with concerning the reduction ratio is designed as follows:

$$\bar{u} = \frac{\hat{K}_{\text{corr}}\tilde{M}(\bar{q})}{(905)(5)}\bar{a}_q + \frac{\tilde{G}(\bar{q})}{905} \tag{13}$$

where

$$\bar{a}_q = \ddot{\bar{q}}^{des} + \hat{K}_d^{ct}\dot{e} + \hat{K}_p^{ct}e \tag{14}$$

4.3 Design of the Independent Joint Controller

The dynamics of the actuation system containing the DC motor and gearhead can be modeled as follows:

$$T = (I_r + \frac{I_L}{N^2})\ddot{\theta}_r + \eta\dot{\theta}_r \tag{15}$$

where I_r, I_L, θ_r, η and N are the rotor's inertia, load's inertia, rotor angular position, viscous friction and reduction ratio, respectively.

As observed in Eq. 15, the effect of the load's inertia on the dynamics is inversely proportional to the reduction ratio. The load's inertia can be neglected in the actuation system's dynamics with a sufficiently high reduction ratio. In NeuRoboScope, the endoscope has a dominant effect on the actuation system. Due to that, the endoscope's inertia around the rotation axis of the actuation system is calculated as $I_L \approx 0.055\ kgm^2$ and $N = 905$. The $\frac{I_L}{N^2} \approx 6.7 \times 10^{-8}\ kgm^2$ is %4 of the $I_r = 14.81 \times 10^{-7}\ kgm^2$. Therefore, the inertia of the load can be neglected in controller design. The independent joint controller is designed as follows:

$$\bar{u} = \hat{K}_d^{ij}\dot{e} + \hat{K}_p^{ij}e + \hat{K}_{corr}\frac{\tilde{G}(\bar{q})}{905} \tag{16}$$

where the PD control parameters ($\hat{K}_d^{ij} = K_d^{ij}\hat{1}$ and $\hat{K}_p^{ij} = K_p^{ij}\hat{1}$) are designed for achieving the desired poles, i.e., $s_{1,2} = -w_n\zeta \pm \sqrt{1-\zeta^2}i$.

5 Experimental Results

The experimental setup is prepared to implement the designed motion controllers as shown in Fig. 7 where the STM32 Discovery board, including the ARM Cortex M4 processor, is used to run the control algorithms at 0.5 kHz. Also, Escon 36/2 DC Servo Controller is used to drive the actuators. Operation mode in Escon 36/2 is set to "speed controller" (open loop) where the control input u is converted to proper control input by using speed/torque gradient coefficient as explained in Maxon Formulae Handbook [35].

During experimental studies, the orientation of the base is fixed at $\theta_4 = -28.5°$ and $\theta_5 = 0°$. The $K_{\text{corr},1}$, $K_{\text{corr},2}$ and $K_{\text{corr},3}$ are obtained from Fig. 4 as 1.84, 1.84 and 2.15, respectively. The performance of the controllers is investigated with three different scenarios, mentioned below, where t shows the time.

1. Initial values: $\phi = 0°$, $\psi = 0°$,$d = 200$ mm.

$$\phi^{des} = 0° \tag{17}$$
$$\psi^{des} = 0° \tag{18}$$
$$d^{des} = \begin{cases} 200 \text{ mm} & t < 10\ s \\ 200 + 50\sin(2\pi 0.1(t-10)) \text{ mm} & t \geq 10\ s \end{cases} \tag{19}$$

2. Initial values: $\phi = 0°$, $\psi = 0°$,$d = 150$ mm.

$$\phi^{des} = \begin{cases} 0° & t < 10\ s \\ 15\sin(2\pi 0.1(t-10))° & t \geq 10\ s \end{cases} \tag{20}$$
$$\psi^{des} = 0° \tag{21}$$
$$d^{des} = 150 \text{ mm} \tag{22}$$

3. Initial values: $\phi = 0°$, $\psi = 0°$,$d = 150$ mm.

$$\phi^{des} = 0 \tag{23}$$
$$\psi^{des} = \begin{cases} 0° & t < 10\ s \\ 20\sin(2\pi 0.1(t-10))° & t \geq 10\ s \end{cases} \tag{24}$$
$$d^{des} = 150\ mm \tag{25}$$

Before the surgeons start to rotate the endoscope about the RCM point P, they insert the endoscope inside the nostril by making a translational motion. In the first scenario, the endoscope's linear travel is arranged so that it captures this whole range of translational motion capability. In the second and third scenarios, 150 mm indicates the condition where the endoscope is inserted all the way inside the nostril. Therefore, the tip point is in the condition where it is located the furthest from the pivot point. This is an actual scenario during the surgical procedure. When the tip point is at the

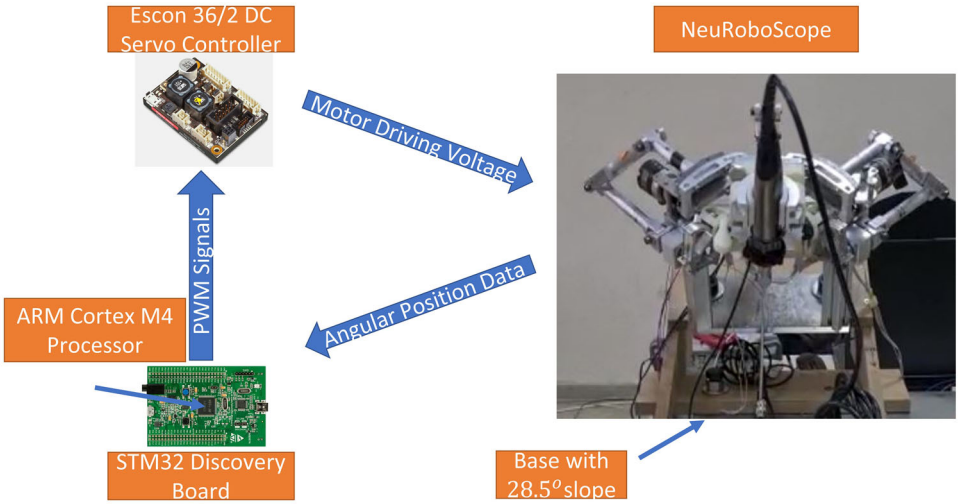

Fig. 7 Experimental setup for the implementation of motion control algorithms in NeuRoboScope

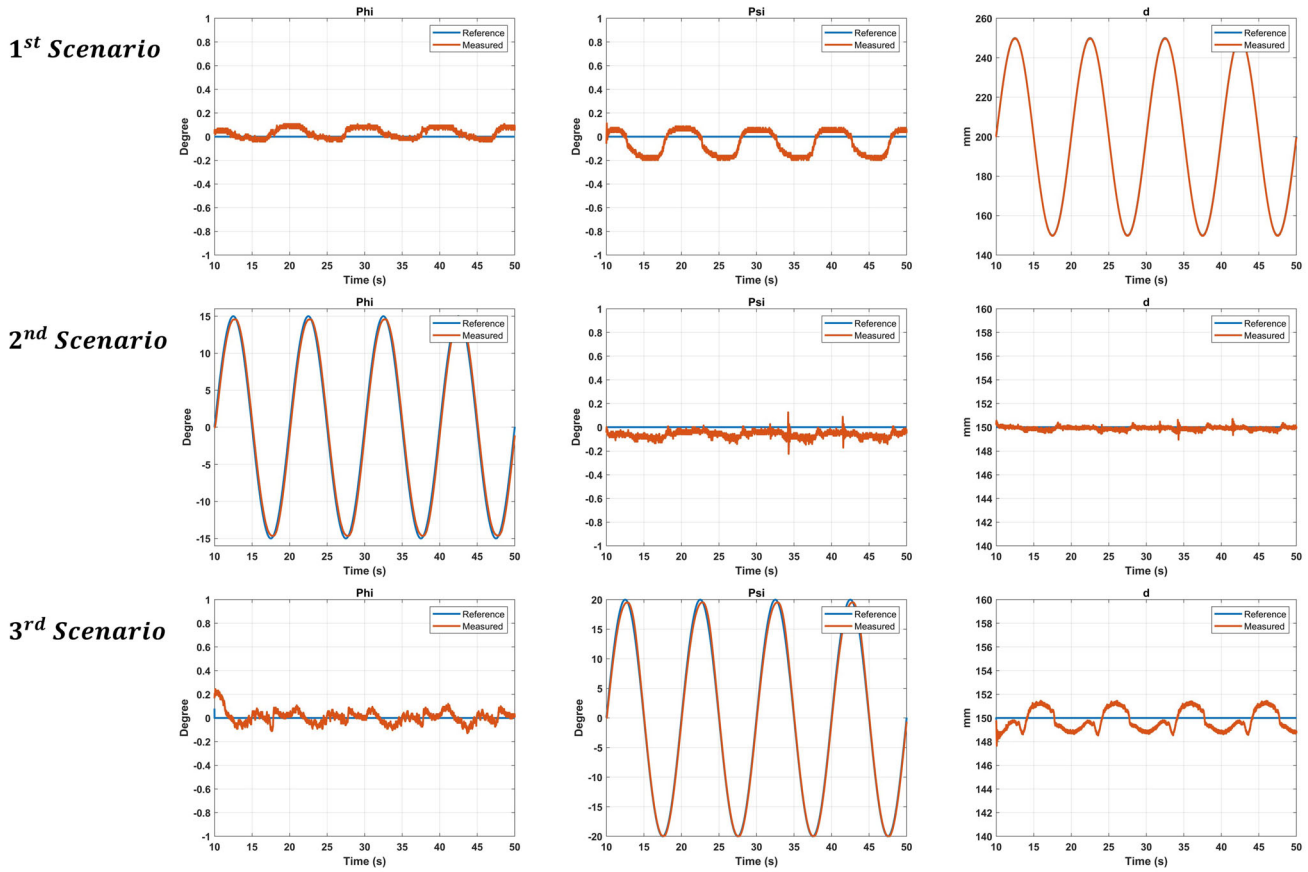

Fig. 8 The results of the experimental studies when implementing the computed torque controller

desired location in terms of the insertion inside the nostril, the surgeon then starts to rotate the endoscope.

By implementing the computed torque controller in Eq. 13 where $K_p^{ct} = 1623.8$ and $K_d^{ct} = 56.9$ are selected according to the actuation dynamics, the results are obtained as indicated in Fig. 8. In the 1^{st} experiment, the sinus wave is given as a reference of d, while ϕ and ψ are kept constant. The RMSEs of ϕ, ψ and d are measured as 0.0515°, 0.1080° and 0.2417 mm, respectively, which are acceptable for the NeuRoboScope system. However, the error of ψ is relatively higher than expected, and the reason is the kinematic relation between ψ and d. This is also observed in 3^{rd} experiment where the RMSE of d ($= 0.8359$ mm) is relatively high, while RMSEs of ϕ, ψ are 0.0511°, 0.7248°,

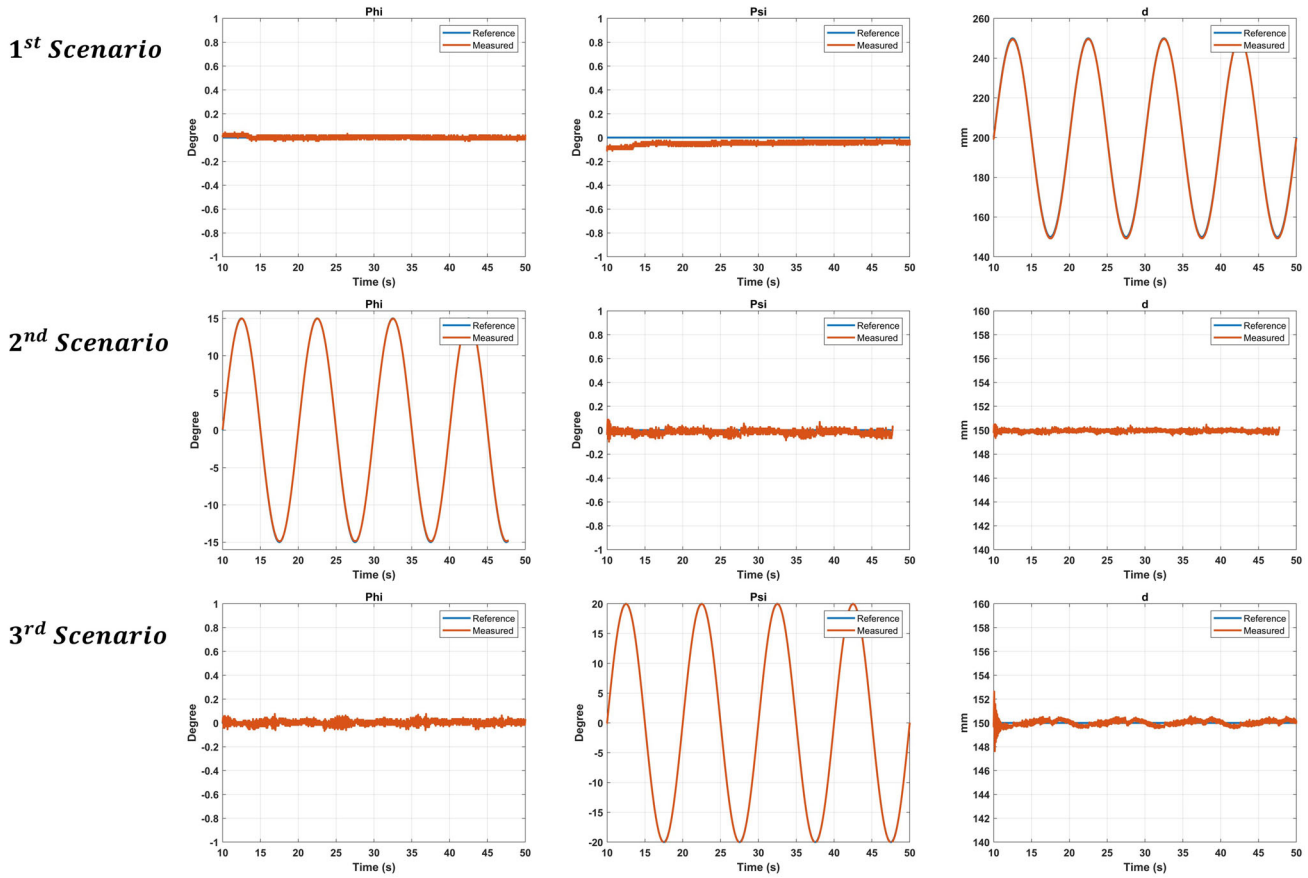

Fig. 9 The results of the experimental studies when implementing the independent joint controller

respectively. In the 2^{nd} experiment, the RMSEs are 0.8216°, 0.0626° and 0.1783 mm where the reference of ϕ is given as sinusoidal and the other task space variables are kept at initial conditions. Moreover, the task space variable following the sinusoidal reference has relatively higher errors, which are acceptable for the NeuRoboScope.

In the design of the independent joint controller in Eq. 16, K_p^{ij} and K_d^{ij} are selected as 0.43 and 0.0076, respectively. The experimental results are presented in Fig. 9 where the RMSEs of 1st, 2^{nd} and 3^{rd} experiments are 0.0124°, 0.0624° and 0.0157° for ϕ, 0.0555°, 0.0279° and 0.0488° for ψ and 0.5122 mm, 0.1261 mm and 0.2224 mm for d, respectively. These are acceptable errors for the NeuRoboScope.

The experimental results indicate that the independent joint controller performs better than the computed torque method with a simplified dynamic model, although the control parameters in both controllers are selected according to the same performance criteria. Also, it is observed that the simplified gravitational acceleration column matrix $\tilde{G}$ used in both controllers can be the substitute for the actual one $\hat{G}$. However, the simplified inertia matrix $\tilde{M}$ does not mimic the actual inertia matrix $\hat{M}$ perfectly.

6 Conclusions

This paper exhibits the design of computationally efficient control methods, which is provided by simplifying the dynamic models of the robot. The simplified dynamic model of the NeuRoboScope is previously studied in [28, 29]. Moreover, the design of the motion control algorithms by using the simplified dynamic model, such as computed torque and independent joint controller, and implementation of them in a novel surgical robot, NeuRoboScope, are presented.

In general, the simulation studies cannot exactly match the behavior of a system that is measured via experimental studies. In this study, the major effects that are not considered in the simulation environment are the joint frictions and the joint clearances. These two are expected to adversely affect the control accuracy of the experimental system when compared to the results obtained via simulations. However, in this study, an actuation system with a high gear ratio is used. Consequently, the major source of friction is at actuation systems. The effect of this friction is taken into account when selecting the controller gains as explained in Section 4. Since the mechanism is an over-constrained parallel mecha-

nism [31], the effect of the joint clearances on the uncertainty of the system is minimized [36].

To evaluate the computational efficiency of the simplified model, the execution time needed for the calculation of the NeuRoboScope's full and simplified dynamic model is measured. The measurement is carried out by using the MATLAB R2019b software, which runs on a laptop computer that has Windows 10 operating system, intel core i7-10750 h processor and 16 GB RAM. For execution time calculation of the NeuRoboScope's full and simplified dynamic model, two functions are created to have the simplified and full dynamic model in which the input and output are actuated joint variables and applied torque by the actuators, respectively. The average execution times of the NeuRoboScope's full and simplified dynamic model are measured to be $\approx 0.011\ s$ and $\approx 0.0016\ s$, respectively. This exhibits that simplified method reduces the computational load on the processor for calculating the NeuRoboScope's dynamic model by almost 7 folds. By using the simplified dynamic model, computed torque control algorithms and independent joint controller with gravity compensation are designed and implemented in the NeuRoboScope's main processor, which is an ARM Cortex M4. Using both motion control algorithms, we were able to execute the control of the actual surgical robot at $0.5\ kHz$ in experimental studies. It is emphasized that the measured execution time on the laptop computer cannot be compared with Arm Cortex M4. In contrast to a laptop computer having Windows 10 operating system, the control algorithm runs in hard real time on the dedicated ARM Cortex M4 microprocessor.

Experimental studies indicate that NeuRoboScope follows the position trajectory with errors in the acceptable range for both control algorithms. Also, it is observed that the independent joint controller has better performance when compared with the computed torque controller, and this demonstrates that the simplified gravitational acceleration matrix mimics the actual one in contrast to simplified inertia matrix. The main reason is that a common correction coefficient is used for the torques generated by inertial and gravitational terms. From Fig. 3, it is known that the dominant effect on the dynamic is the gravitational terms for that reason; the correction coefficient cannot be properly designed for inertial torques. In future studies, the correction coefficient for the simplified inertia matrix and simplified gravitational acceleration matrix will be derived independently.

Acknowledgements This work was supported in part by The Scientific and Technological Research Council of Turkey via grant number 219M483.

Author Contributions The study was designed by OA and Mehmet İsmet Can Dede. Material preparation and data collection were performed by OA. The data analysis was performed by OA and supervised by MİCD. The first draft of the manuscript was written by OA and revised by MCD. All authors read and approved the final manuscript.

Funding This study was supported by a grant of 219M483 funded by The Scientific and Technological Research Council of Turkey (TÜBİTAK). The funders had no role in study design, data collection, analysis, and interpretation, or preparation of the manuscript.

Data availability statement Data sharing was not applicable to this article as no datasets were generated or analyzed during the current study

Declarations

Conflicts of interest Orhan Ayit and Mehmet İsmet Can Dede declare that they have no competing interests

References

1. Jaffray B (2005) Minimally invasive surgery. Arch Disea Child 90(5):537–542
2. Miscusi M, Polli FM, Forcato S, Ricciardi L, Frati A, Cimatti M, De Martino L, Ramieri A, Raco A (2015) Comparison of minimally invasive surgery with standard open surgery for vertebral thoracic metastases causing acute myelopathy in patients with short-or mid-term life expectancy: surgical technique and early clinical results. J Neurosurg: Spine 22(5):518–5252
3. Knott L. Minimally invasive surgery (2013) Published at https://patient.info/doctor/minimally-invasive-surgery
4. Hanna GB, Cuschieri A (2008) Ergonomics of task performance in endoscopic surgery. In: Bax KMA, Georgeson KE, Rothenberg SS, Valla J, Yeung CK (eds) Endosc Surg Infants Child. Heidelberg, New York, Berlin, pp 39–50
5. Köckerling F (2014) Robotic vs standard laparoscopic technique - what is better? Front Surg 1:1–15
6. Wee IJY, Kuo LJ, Ngu JCY (2020) A systematic review of the true benefit of robotic surgery: ergonomics. Int J Med Robot Comput Assisted Surg 16:e2113
7. Hurley AM, Kennedy PJ, O'Connor L, Dinan TG, Cryan JF, Boylan G, O'Reilly BA (2015) Sos save our surgeons: stress levels reduced by robotic surgery. Gynecol Surg 12(3):197–206
8. Acıbadem Web and Medical Content Editorial Board. Robot-assisted surgery, (2020). Published at https://www.acibadem.com.tr/en/in-acibadem/robot-assisted-surgery/
9. Attanasio A, Scaglioni B, De Momi E, Fiorini P, Valdastri P (2021) Autonomy in surgical robotics. Annual Rev Cont, Robot Autonom Syst 4:651–679
10. Broeders, I.A.M.J. and Ruurda, J (2001), "Robotics revolutionizing surgery: the Intuitive Surgical "Da Vinci" system", Industrial Robot, Vol. 28 No. 5, pp. 387–392
11. Beasley, R. A (2012). Medical robots: Current systems and research directions. Journal of Robotics, 2012
12. Broeders I. A. M. J. and Ruurda J 92001) Robotics revolutionizing surgery: the intuitive surgical "da vinci" system. Ind Robot: an Int J,
13. Beasley R. A (2012) Medical robots: current systems and research directions. J Robot
14. Gosrisirikul C, Chang KD, Raheem AA, Rha KH (2018) New era of robotic surgical systems. Asian J Endoscopic Surg 11(4):291–299
15. Featherstone, R (1984) Robot dynamics algorithms [Doctoral thesis, University of Edinburgh]. Edinburgh Research Archeive. http://hdl.handle.net/1842/18179

16. Zhang Z, Zhang L, Yang GZ (2017) A computationally efficient method for hand-eye calibration. Int J Comput Assisted Radiol Surg 12(10):1775–1787
17. Bogatyrenko E, Pompey P, Hanebeck UD (2011) Efficient physics-based tracking of heart surface motion for beating heart surgery robotic systems. Int J Comput Assisted Radiol Surgery 6(3):387–399
18. Featherstone R. Robot dynamics algorithms. *Annexe Thesis Digitisation Project 2016 Block 5*, 1984
19. Du J. and Lou Y (2016) Simplified dynamic model for real-time control of the delta parallel robot. In : 2016 IEEE International conference on information and automation (ICIA), pp. 1647–1652. IEEE,
20. Brinker J., Ingenlath P., and Corves B (2018) A study on simplified dynamic modeling approaches of delta parallel robots. In: Advances in Robot Kinematics 2016, pp 119–128. Springer
21. Ayit O., Yasir A., Vardarli E., Kiper G., and Dede M. I. C (2018) Bir ameliyat robotunun denetimi için basitlestirilmis dinamik modeli. In: Otomatik Kontrol Ulusal Toplantisi (TOK), pp. 265–270
22. Wang K., Léonard F., and Abba G (2014) A novel approach for simplification of industrial robot dynamic model using interval method. In 2014 IEEE/ASME International Conference on Advanced Intelligent Mechatronics, pp. 1697–1703. IEEE
23. Yasir A (2018) Design of a 2R1T mechanism with remote center of motion for minimally invasive transnasal surgery applications [Doctoral thesis, Izmir Institute of Technology]. ProQuest Dissertations & Theses Global
24. Carbonari L (2015) Simplified approach for dynamics estimation of a minor mobility parallel robot. Mechatronics 30:76–84
25. Zhang X, Fan B, Wang C, Cheng X (2021) Analysis of Singular Configuration of Robotic Manipulators. Electronics 10(18):2189
26. Guoqin G., Mengchun Z., and Zhida B (2016) Dynamic modeling and sliding mode control of a novel parallel mechanism. In 2016 12th IEEE International Conference on Control and Automation (ICCA), pp. 785–790. IEEE
27. Ogata, K (2004). System Dynamics (4th ed.). Pearson
28. Ayit O., Yaşır A., Vardarlı E., Kiper G., and Dede M. İ. C (2018) Bir ameliyat robotunun denetimi için basitleştirilmiş dinamik modeli. TOK 2018 Bildiriler Kitabı,
29. Ayit O, Dede MİC (2021) A new correction coefficient formula for the simplified dynamic model of a surgical robot. In: Rauter G, Cattin PC, Zam A, Riener R, Carbone G, Pisla D (eds) New trends in medical and service robotics. Cham, Springer International Publishing, pp 89–96
30. Yaşır A (2018) Design of a 2R1T mechanism with remote center of motion for minimally invasive transnasal surgery applications. PhD thesis, Izmir Institute of Technology (Turkey)
31. Yaşır A, Kiper G, Dede MİC (2020) Kinematic design of a non-parasitic 2r1t parallel mechanism with remote center of motion to be used in minimally invasive surgery applications. Mech Mach Theory 153:104013
32. Zhang X., Fan B., Wang C., and Cheng X (2021) Analysis of singular configuration of robotic manipulators. Electronics, 10(18)
33. Maaroof O. W. N (2020) Design of a robot assisted minimally invasive surgical system for pituitary tumor surgery based on safety features. PhD thesis, Izmir Institute of Technology (Turkey)
34. Ogata K (1978) System dynamics. Englewood Cliffs
35. Braun J (2012) Formulae handbook. Maxon Academy, Sachseln. First Edit. Maxon Motor by Precision, pp 1–60
36. Merlet JP (2006) Parallel robots,128. Springer Science & Business Media, New York